

What is the Limit Size of 2D Conjugated Extension on Central Units of Small Molecular Acceptors in Organic Solar Cells?

Xingqi Bi, Xiangjian Cao, Tengfei He, Huazhe Liang, Zhaoyang Yao,* Jinyi Yang, Yaxiao Guo,* Guankui Long, Bin Kan, Chenxi Li, Xiangjian Wan, and Yongsheng Chen*

2D conjugated extension on central units of small molecular acceptors (SMAs) has gained great successes in reaching the state-of-the-art organic photovoltaics. Whereas the limit size of 2D central planes and their dominant role in constructing 3D intermolecular packing networks are still elusive. Thus, by exploring a series of SMAs with gradually enlarged central planes, it is demonstrated that, at both single molecular and aggregated levels, there is an unexpected blue-shift for their film absorption but preferable reorganization energies, exciton lifetimes and binding energies with central planes enlarging, especially when comparing to their Y6 counterpart. More importantly, the significance of well-balanced molecular packing modes involving both central and end units is first disclosed through a systematic single crystal analysis, indicating that when the ratio of central planes area/end terminals area is no more than 3 likely provides a preferred 3D intermolecular packing network of SMAs. By exploring the limit size of 2D central planes, This work indicates that the structural profiles of ideal SMAs may require suitable central unit size together with proper heteroatom replacement instead of directly overextending 2D central planes to the maximum. These results will likely provide some guidelines for future better molecular design.

the best power conversion efficiency (PCE) of OSCs still lags far behind the state-of-the-art crystalline silicon or perovskite solar cells.^[3] Intrinsically, the inherent weaker intermolecular Van de Waals interaction (rather than covalent bonds) and higher packing disorder of organic light-harvesting materials compared with their inorganic counterparts should be responsible for this huge gap of PCEs.^[4] The lacking strength of intermolecular interaction and crystalline ordering will inevitably result in 1) localized excitons possessing a small radius less than 1 nm and large binding energy over 0.3 eV.^[5] In this way, the efficient exciton diffusion via the Förster and Dexter energy transfers,^[6] meanwhile, exciton dissociation at small driving forces will be impeded;^[7] 2) insufficient overlap of p-orbital electron clouds between adjacent molecules, which leads to inferior charge migration through a hopping mechanism; 3) large lattice imperfection or non-crystalline phase hidden in aggregations

of organic molecules, affording to lots of scattering/recombination sites for excitons and electrons.^[2d,8] These disadvantages are much intertwined and further result in much low carrier mobilities and quite severe charge recombination,^[2j,9] thus unsatisfied PCEs of OSCs. Therefore, how to strengthen intermolecular stackings, meanwhile, improve molecular

1. Introduction

Organic solar cells (OSCs) have achieved significant developments in the past five years and are likely on the eve of industrial application currently,^[1] which mainly benefits from the innovative exploration of small molecular acceptors (SMAs).^[2] However,

X. Bi, X. Cao, T. He, H. Liang, Z. Yao, J. Yang, C. Li, X. Wan, Y. Chen
State Key Laboratory and Institute of Elemento-Organic Chemistry
Frontiers Science Center for New Organic Matter
The Centre of Nanoscale Science and Technology and Key Laboratory of
Functional Polymer Materials
Renewable Energy Conversion and Storage Center (RECAST)
Tianjin Key Laboratory of functional polymer materials
College of Chemistry
Nankai University
Tianjin 300071, China
E-mail: zyao@nankai.edu.cn; yschen99@nankai.edu.cn

Y. Guo
State Key Laboratory of Separation Membranes and Membrane
Processes
School of Chemistry
Tiangong University
Tianjin 300387, China
E-mail: yaxiaoguo@tiangong.edu.cn
G. Long, B. Kan
School of Materials Science and Engineering
National Institute for Advanced Materials
Renewable Energy Conversion and Storage Center (RECAST)
Nankai University
Tianjin 300350, China

 The ORCID identification number(s) for the author(s) of this article can be found under <https://doi.org/10.1002/sml.202401054>

DOI: 10.1002/sml.202401054

crystalline ordering should be a very crucial but quite challenging issue for developing more efficient organic photoelectric materials.^[20,10]

With the aim of addressing above challenges, our group has developed a series of CH SMAs recently.^[10a,11] Their most notable feature is 2D conjugated extension of central units, which provides sufficient chemical modification sites on molecular backbones to tune molecular packing behaviors.^[12] What excites us greatly is the strength of and packing ordering can be significantly enhanced because of dual effects of stronger π - π packings and newly emerged noncovalent bonds of X...H, X...S, X... π , etc.^[10a,13] In this way, the vibration of photo-generated excitons could be largely delocalized on neighboring well-stacked molecules,^[2d,14] which will lead to prolonged exciton lifetimes, decreased exciton binding energies, weakened electron-vibration coupling between charge transfer and ground states.^[15] Consequently, these advantages could work together to afford much facilitated charge migration and suppressed recombination,^[10a,16] further dramatically improve photovoltaic performances of OSCs. Although the dominant role of halogenated 2D conjugated central units in molecular packings and even photovoltaic performance has been preliminarily unveiled,^[11] the limit exploration of 2D conjugated extension on central units, like the most suitable plane size/ratio or underlying structural elements, is still rather elusive, bringing about the absence of clear structure-activity currently for CH-series SMAs.

In order to reveal the structure-function relationship between 2D conjugated central plane of SMAs and their characteristic 3D intermolecular packing networks, even quite different efficiency of resulting OSCs, a series of high-performance SMAs (CH20, CH50, CH70 in Figure S1 (Supporting Information) and their bromides of CH22, CH52, and CH72 in Figure 1a) were constructed with gradually enlarged central units,^[13] for example the projected area of central units being ≈ 8.5 for Y6, ≈ 15.3 for CH20/CH22, ≈ 23.7 for CH50/CH52, and ≈ 30.6 Å² for CH70/CH72. Surprisingly, gradually blue-shifted absorption has been observed for their film states, however, smaller reorganization energies, prolonged exciton lifetimes and reduced binding energies are achieved comparing to their Y6 counterpart. More interesting and importantly, by a systematic single crystal analysis of these molecules, a proper ratio of central plane projected area (S_C)/end terminal projected area (S_E) with no more than 3 was disclosed, indicating the great significance of multiple and well-balanced molecular packing modes involving both central and end units for a more preferred 3D intermolecular packing network for SMAs. Thus, by exploring the limit/proper size of 2D conjugated planes of central unit and property-structure relationship, our work has elucidated the structural profiles of optimal central unit that well-meet the design criterion of high-performance SMAs.

2. Results and Discussion

2.1. Synthesis and Characterization

The synthetic routes to SMAs that involving with a key step of condensation^[10a] were exhibited in Scheme S1–S5 (Supporting Information). The synthesized/characterized details were presented in Figures S25–S52 (Supporting Information). Due to

the similar structures and varying tendency of physico-chemical properties between CH20, CH50, CH70 and their bromides, together with the relatively higher performance of the bromides (see below), we just made a detailed comparison of CH22, CH52, and CH72 for the clarification of discussions.^[17]

In spite of the greatly enlarged 2D conjugated extension on central units, all the SMAs (including Y6 counterpart) still show the desired planar geometries (Figure S2, Supporting Information) and featured A-D-A structures^[2b,18] along the longest molecular backbone (Figure 1b) based on the related density functional theory (DFT) calculations. Therefore, the highest occupied molecular orbitals (HOMOs) and lowest unoccupied molecular orbitals (LUMOs) distribute along the whole molecular skeletons (Figure S3, Supporting Information) with the greatest probability on central donors and two electron-withdrawing terminals, respectively, implying a strong intramolecular charge transfer (ICT).^[18] According to DFT simulations, CH22, CH52, and CH72 afford a very similar bandgap of ≈ 2.05 eV to the well-known Y6 at the single molecular level (Figure S3, Supporting Information). As expected, the almost identical UV-vis spectra profiles of CH22, CH52, and CH72 in solutions can be observed, bathochromically shifted by less than 10 nm comparing to that of Y6 (Figure 1c). Additionally, as shown in Figure S4 (Supporting Information), with the central unit enlarging, solutions of CH52 and CH72 show larger molar extinction coefficients than CH22 (2.68×10^5 for CH22, 4.50×10^5 for CH52, 3.41×10^5 m⁻¹ cm⁻¹ for CH72), demonstrating the enhanced light harvesting capacity of CH52 and CH72 with central planes enlarging.

The calculated isotropic polarizability of central unit increases gradually with its enlarged unit size, being 185.01, 274.86, and 316.09 Bohr³ for the central units of CH22, CH52, and CH72, respectively (Figure 1d). Therefore, it is also plausible to observe stepwise enlarged polarizability from CH22 to CH72, all of which are larger than that of Y6. The larger polarizability of SMAs may theoretically contribute to a decreased intrinsic exciton binding energy (E_b).^[4b,19] As displayed in Figure 1e, an E_b of 1.73 meV is afforded by Y6 by using theoretically prediction in gas phase, whereas an obviously smaller one of 1.62 meV can be rendered by CH22. With the plane expansion of central units, the E_b further decreases to 1.60 meV for CH52 and 1.59 meV for CH72. The gradually reduced E_b is expected to contribute to more effective exciton delocalization and guarantee efficient exciton dissociation driven by a highly small driving force.^[7] Of particular note is that E_b varies greatly with different solid-state polarization effects, intermolecular packing modes and electronic interactions of SMAs.^[4b,12,15f] Thus the presented E_b s above only give clue to the positive effects of 2D conjugated extension of central units at single molecular levels. Furthermore, the reorganization energies of SMAs were also calculated and illustrated in Figure 1f. Both the electron (148.9, 135.2, and 138.2 meV for CH22, CH52, and CH72, respectively) and hole (178.6, 174.0, and 174.6 meV for CH22, CH52, and CH72, respectively) reorganization energies of CH-series SMAs become smaller than those of Y6 (151.0 meV for electrons and 181.5 meV for holes), roughly agreeing with their Stokes shift variations in diluted solutions (Figure 1c,e). The decreased reorganization energies of CH-series SMAs should be attributed mainly to their enlarged conjugation in the central units. Note that CH-series SMAs also have more rigid molecular backbones that mainly afforded by the

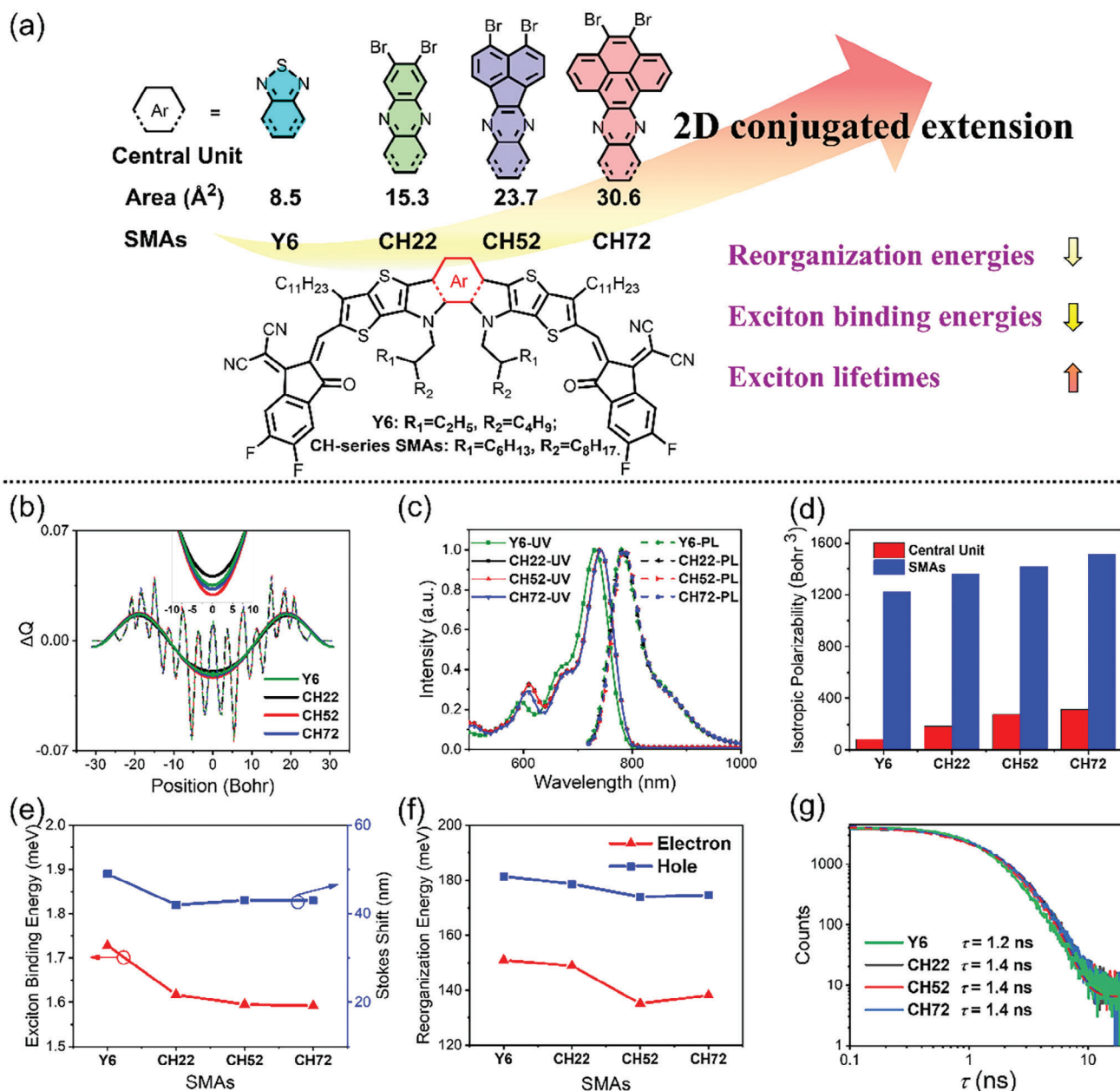


Figure 1. a) Structures and design methodology of SMAs with 2D conjugated central units. b) Charge density difference (ΔQ) of frontier molecular orbitals. c) Normalized ultraviolet-visible (UV-vis) and photoluminescence (PL) spectra of SMAs in solutions. d) Theoretical isotropic polarizability of central units and SMAs. e) Theoretical exciton binding energies of SMAs in gas phase and Stokes shifts in solutions. f) Theoretical reorganization energies of SMAs. g) Time-resolved PL decay traces of SMAs in solutions.

strong non-covalent S-N secondary interaction between nitrogen on phenazine and sulfur on neighboring thiophene (discussed in detail below).^[10d,12] The more planar and rigid skeletons of CH-series SMAs are expected to weaken the electron-vibration coupling between local exciton (LE) or charge transfer (CT) states and their ground states (GS), furthermore, suppress the non-radiative recombination from CT states.^[15b,c] Consequently, it is reasonable to see a slightly larger exciton lifetime of 1.4 ns for 2D conjugated CH-series SMAs than that of 1.2 ns for their Y6 counterpart (Figure 1g).

To sum up, at single molecular levels of SMAs (indicated by their features in diluted solutions or DFT calculations in gas phase), the 2D conjugated extension of central units could result in several preferable variations of physico-chemical properties including red-shifted absorptions, smaller reorganization energies, prolonged exciton lifetimes, reduced binding energies, etc. However, due to the greatly enlarged plane size of central units, the intermolecular packing behaviors of SMAs, such as packing modes, π - π stacking distances and topological structures of 3D packing network, should be much different. That is to say, the

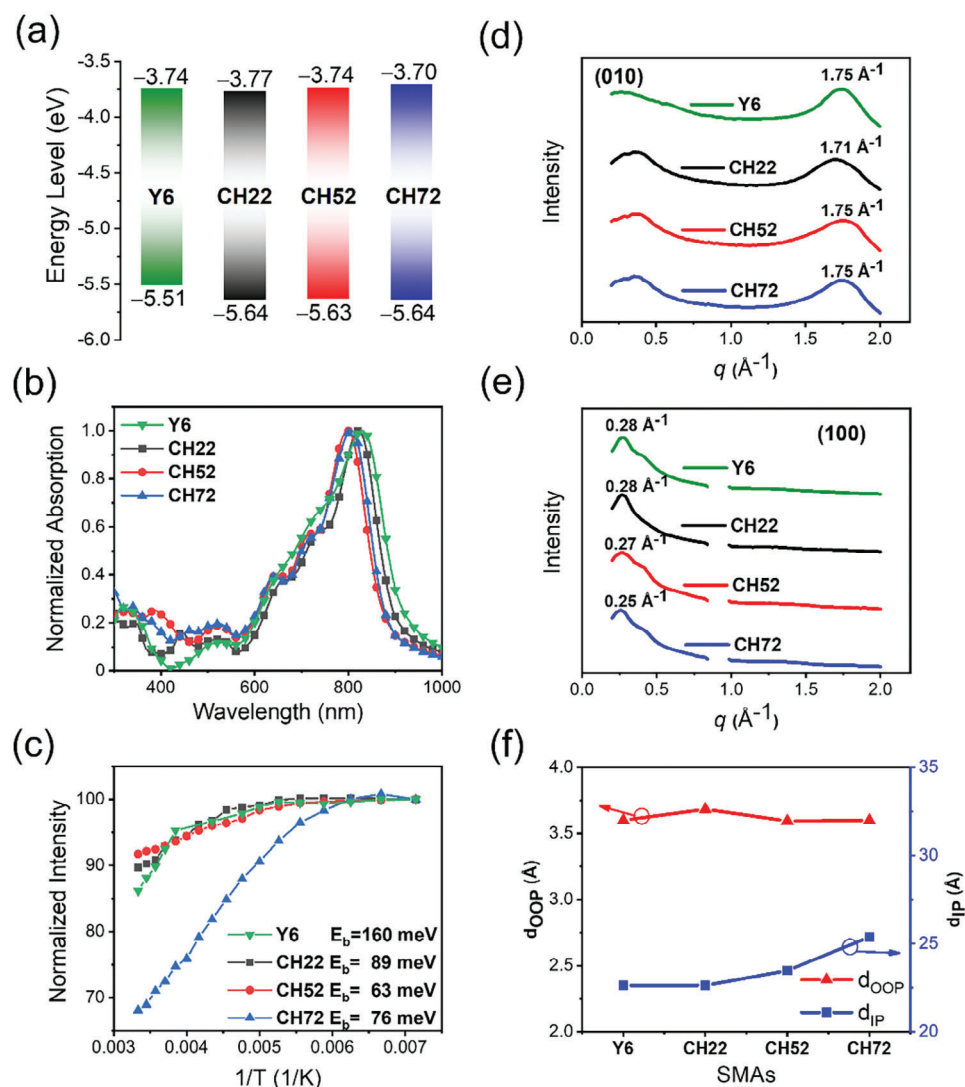


Figure 2. a) Energy levels derived from CV measurements. b) UV-vis spectra in solid films. c) E_b derived from temperature-dependent PL spectra. d,e) Line-cut profiles of 2D GIWAXS patterns of neat films. f) Stacking distance of SMAs in OOP and IP directions.

desired properties of SMAs in solutions or gas phases, which benefits for organic photovoltaic devices, may be not fully maintained or matter in their aggregated states, especially when considering the complexity of organic molecular aggregations. That is why the properties of SMAs in solid films have been further investigated extensively and fully discussed below.

The HOMO/LUMO energy levels of Y6, CH22, CH52, and CH72 in their solid films are $-5.51/-3.74$, $-5.64/-3.77$, $-5.63/-3.74$, and $-5.63/-3.70$ eV, respectively, based on cyclic voltammetry (CV) measurements (Figure 2a; Figure S5, Supporting Information). Therefore, the energy gaps are calculated as 1.77 for Y6, 1.87 for CH22, 1.89 for CH52, and 1.94 eV for CH72. It is interesting that the varying tendency of energy gap is much different from the theoretical calculations in gas phase. When taking the different plane sizes of central unit into consideration, the derived diverse intermolecular packing behaviors of four SMAs, like different packing modes that prefer to forming J- or H-aggregations,^[20] should account for the gradually enlarged en-

ergy gap from Y6 to CH72. As a consequence, the stepwise blue-shifted absorptions

from Y6 to CH72 can be also observed in their solid states (Figure 2b), demonstrating that the maximum extension of central units may be not a good choice if attempting to improve the near-infrared light harvesting capacity of SMAs. Moreover, by analyzing the temperature-dependent PL spectra of neat films, an E_b of 89 for CH22, 63 for CH52, and 76 meV for CH72 can be observed, which are significantly smaller than that of 160 meV for Y6 (Figure 2c; Figure S6, Supporting Information). Therefore, three inferences can be concluded as following: 1) The E_b s of SMAs derived from temperature-dependent PL are much smaller than those predicted by DFT calculations. This mismatch is mainly caused by the significantly enhanced solid-state polarization and intermolecular electronic coupling varying from gas phase to aggregation.^[19] 2) The significantly reduced E_b s of CH-series SMAs have demonstrated the obvious advantage over their Y6 counterpart, endowing with

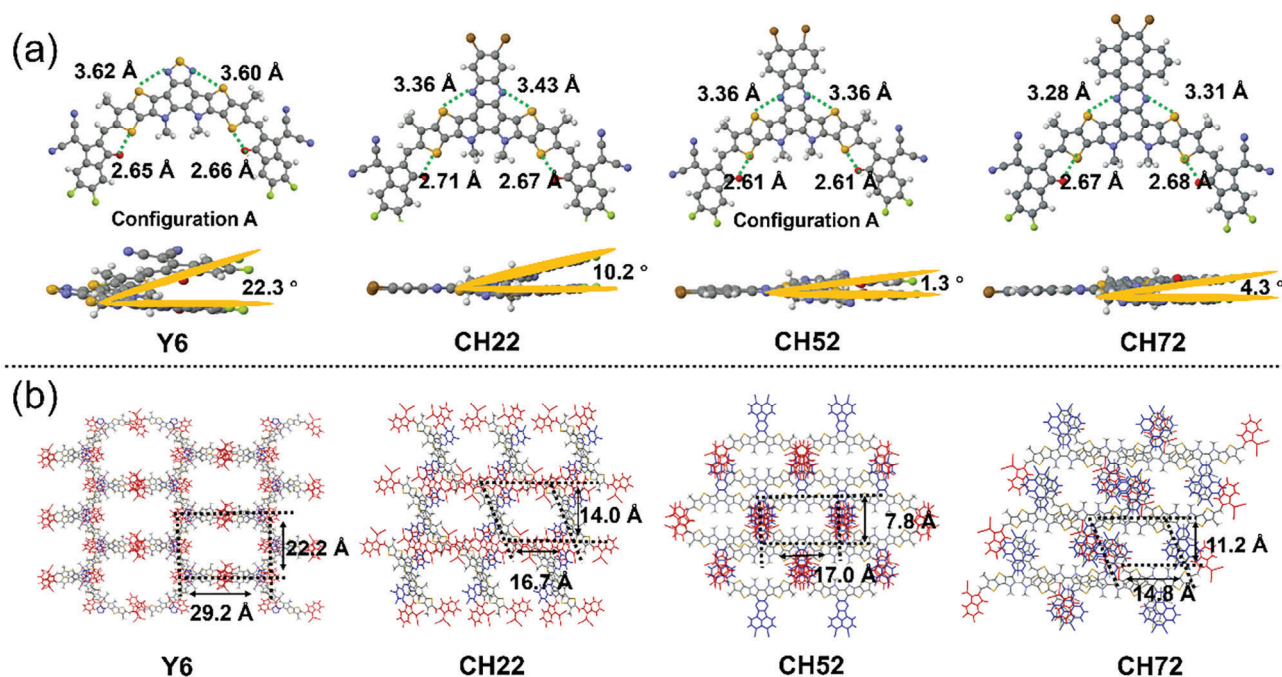


Figure 3. a) Monomolecular single crystallographic structures of Y6, CH22, CH52, and CH72 from top-view and side-view (the alkyl chains are omitted for clarity). The dihedral angles between two end units were also indicated. b) 3D single-crystal packing topological structures on the top view.

CH-series SMAs the great potential to reach efficient exciton dissociations even with a quite small driving force.^[4b] 3) Last but definitely not least is that E_b s of SMAs could be successfully tuned and decreased through conjugation expansion of central units. This feature makes organic SMAs highly possible to achieve an E_b approaching that of inorganic semiconductors if delicate optimization of central unit structures can be performed.

Then, we further performed grazing-incidence wide-angle X-ray scattering (GIWAXS) measurements to shed light on the influences of central plane sizes on molecular stacking strength and ordering (Figure S7 and Table S5, Supporting Information).^[21] All the four SMA neat films displayed a desired face-on packing orientation, suggested by the sharp (010) and (100) peaks in out-of-plane (OOP) and in-plane (IP) directions, respectively (Figure 2d,e). The (010) peaks in OOP direction located at 1.75 for Y6, 1.71 for CH22, 1.75 for CH52, and 1.75 \AA^{-1} for CH72 films (Table S5, Supporting Information), corresponding to π - π stacking distances ($d_{\pi-\pi}$) of ca. 3.60, 3.68, 3.59, and 3.60 \AA , respectively (Figure 2f). Because of the enlarged alkyl substituents on CH22 comparing to Y6, CH22 demonstrates a relatively larger $d_{\pi-\pi}$ of 3.68 \AA than that of 3.60 \AA for Y6. With the plane size of central units increasing, CH52 and CH72 afford a greatly decreased $d_{\pi-\pi}$ of ≈ 3.60 \AA comparing to that of CH22, suggesting that the large central unit planes of CH52 and CH72 become deeply involved in molecular packings of SMAs (see detailed discussions in section of single crystal analysis). Note that the more compact molecular π - π stackings are expected to delocalize the photogenerated excitons on adjacent stacked SMAs efficaciously,^[14a] thus giving rise to the reduced exciton binding energies of SMAs in solid states.^[11]

2.2. Molecular Packing in Single Crystals

As it has been discussed above, the plane size of central units may play a crucial role in molecular packing behaviors of SMAs.^[12,22] Therefore, single-crystal X-ray diffraction characterization of SMAs including CH50/CH52 and CH70/CH72 were performed. In addition, the single crystals of Y6 and CH20/CH22 were also accessed from literatures^[4c,13] and a systematic analysis has been conducted in order to reveal the great role of central unit in determining molecular geometries and intermolecular packing modes. By using a slow solvent diffusion method (see Supporting Information for the details), single crystals of CH50/CH52 and CH70/CH72 were afforded. In light of the similar molecular structures and intermolecular packing behaviors between CH20, CH50, CH70 and their bromides of CH22, CH52, CH72, we just compared the crystals of CH22, CH52, and CH72 in detail below for clarity. But the corresponding single crystal structures and parameters of CH20, CH50, and CH70 were also presented in Figures S8–S10 and Tables S6–S8 (Supporting Information).

As shown in Figure 3a, all the SMAs of Y6, CH22, CH52, and CH72 display an alike banana-shape and helical geometry. Among them, Y6 and CH52 possess two configurations, whereas CH22 and CH72 have only one (Figure S11, Supporting Information). The torsion angles between two planes built from two end units can be used to assess the planarity of molecular backbones, being 22.4° for Y6, 10.2° for CH22, 1.3° for CH52 and 4.25° for CH72, which shows the roughly similar tendency to their DFT calculated geometries (Figure S12, Supporting Information). It is really interesting that the torsion angles of CH-series SMAs are much smaller than that of Y6, resulting in much better molecular planarity and rigidity for CH-series SMAs. The root cause of advantages above could be ascribed to the strong non-covalent S-N

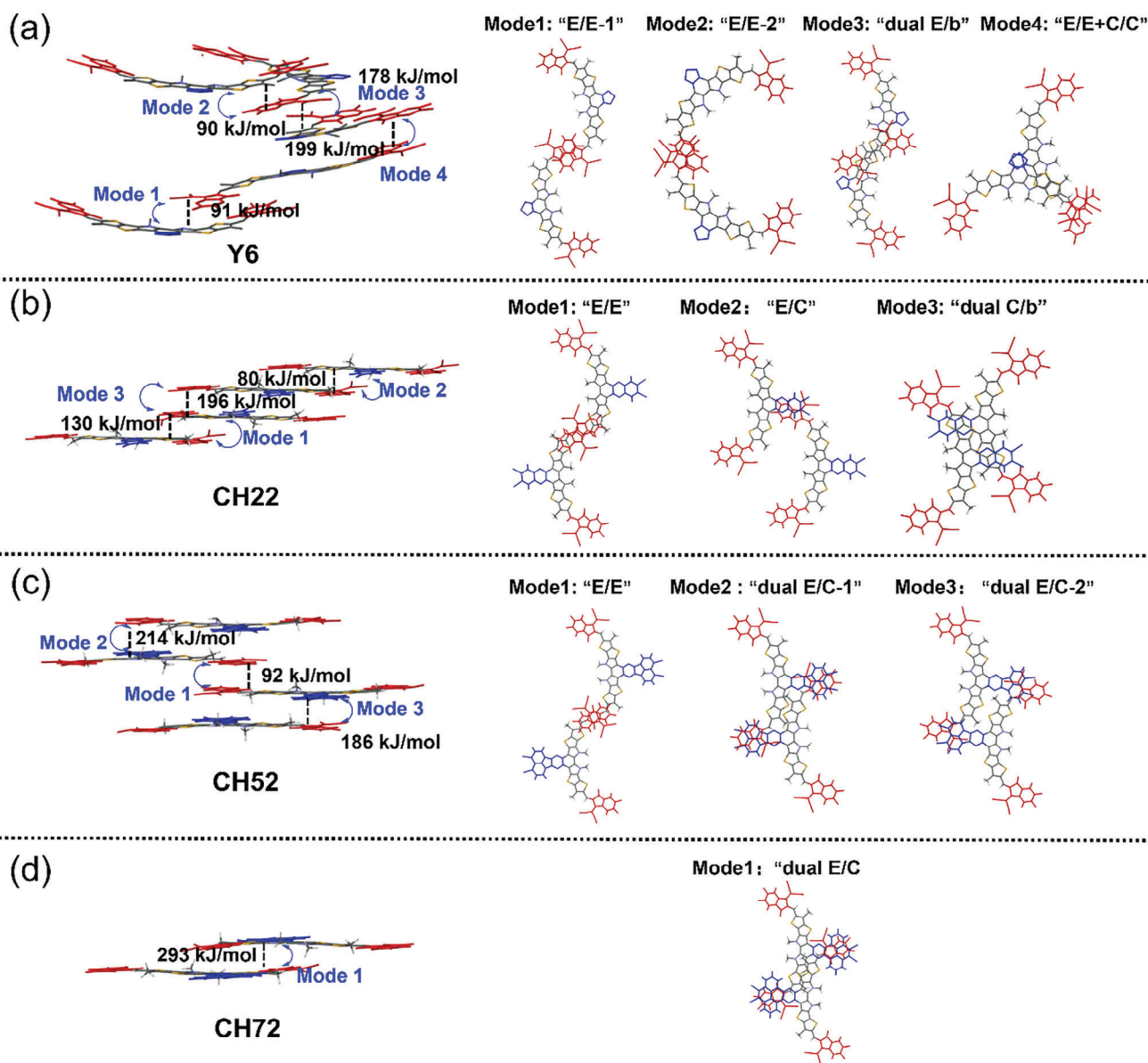


Figure 4. Intermolecular potentials including all the corresponding intermolecular packing modes. a) Y6; b) CH22; c) CH52; d) CH72. Herein, the E, b and C represent end, bridge, and central units, respectively.

secondary interaction between nitrogen on phenazine and sulfur on neighboring thiophene bridges. This non-covalent bond is widely showed in CH-series SMAs and featured with an N-S van der Waals distance of ≈ 3.35 Å, smaller than the non-bonding distance of ≈ 3.50 Å.^[10d,12] Based on the topological structures of single crystal (Figure 3b), different plane sizes of central nucleus have resulted in dramatically different intermolecular packing networks. The single crystal of Y6, which is assigned to a monoclinic system with rectangle-shaped voids of $\approx 22.2 \times 29.2$ Å, has proven the unique role of central units in constructing desired 3D intermolecular packing networks.^[4c,12] When extending the central plane of SMAs stepwise, the excellent 3D intermolecular stacking networks could be well maintained with much smaller void sizes ($\approx 16.7 \times 14.0$ for CH22; $\approx 17.0 \times 7.8$

for CH52; $\approx 14.8 \times 11.2$ Å for CH72) but assigned to different crystalline systems (triclinic for CH22; monoclinic for CH52; triclinic for CH72). As expected, the plane size of central units in SMAs could tune the molecular packing behaviors greatly, thus resulting in different crystalline systems and multidimensional intermolecular stacking networks, which may further exert positive or negative effects on charge transfer/transport dynamics in photovoltaic devices.

Intrinsically, the obvious differences of crystal frameworks for Y6, CH22, CH52, and CH72 should originate from the diverse intermolecular packing modes. Therefore, the main packing modes with intermolecular potentials $>|70|$ kJ mol⁻¹ have been extracted and presented in Figure 4. The typical Y6 possesses four packing modes, including two "end unit to end unit" (E/E-1/2),

one “dual end unit to bridge unit” (dual E/b) and one “end unit to end unit and central unit to central unit” (E/E+C/C), all of which work together and establish the superior 3D intermolecular stacking network of Y6.^[4c] Among them, the “E/E+C/C” mode with a large intermolecular potential of -199 kJ mol^{-1} has been regarded as the unique packing style first observed in Y-series acceptors, moreover, may play the most important role in boosting molecular packing transformation from 2D to 3D.^[10a] As regards to CH22, the most common packing mode of “E/E” in SMAs still can be observed in spite of the central unit extension. However, two newly formed packing modes of “end unit to central unit” (E/C) and “dual central unit to bridge unit” (dual C/b) are afforded with the relatively large intermolecular potentials of -80 and -196 kJ mol^{-1} , respectively. Their features in common are that the central unit is greatly involved with molecular packings due to its dramatically 2D conjugated extension. When further enlarging the plane size of central unit in CH52, the π - π interaction strength between two main planar segments (central and end units) in molecular backbone is enhanced significantly, thus giving rise to two similar but newly formed packing modes of “dual end unit to central unit” (dual E/C-1/2) besides that of “E/E”. It is obvious that the stacking mode involving 2D central unit is becoming more thermodynamically stable (indicated by their much larger intermolecular potentials of -214 and -186 kJ mol^{-1} comparing to that of -92 kJ mol^{-1} for “E/E” mode in CH52) and plays a dominant role in establishing the 3D crystallographic structure of CH52. Note that a similar trend can be also observed in single crystal of CH50. In a similar fashion, by further extending central unit to the maximum, the packing mode of “E/E” that widely exists and even dominates in ITIC- and Y-series SMAs, vanishes from sight in CH72. More interestingly, only one packing mode of “dual E/C” can be observed in CH72 with the largest intermolecular potential of -271 kJ mol^{-1} . The huge central unit plane in CH72 may provide an overwhelming driving force to prompt the formation of “dual E/C” packing modes rather than “E/E” mode, thus making “dual E/C” mode completely dominate the stacking of CH72. In addition, as shown in Figure S10 (Supporting Information), with the same size of central unit, single crystals of CH70 show the same trend as that of CH72.

As we have illustrated above, the intermolecular potentials of main packing modes in SMAs are increased with the conjugation extension of central units. When extending the central unit plane to the maximum, CH70 and CH72 even exhibits only one molecular stacking mode with the largest intermolecular potential. This may help to reduce the disorder of molecular stacking and obtain better charge transport/recombination dynamics in theory. However, a positive correlation is not observed yet between the efficiency of photovoltaic devices (discussed in detail below) and the projected area of central planes. Therefore, we speculate that the contribution of different stacking modes to intermolecular charge transfer should be particularly different. Given the molecules herein studied are working as electron transporting materials, the electron transfer integrals (V_E) of different packing modes were calculated to estimate the overall charge transport ability of SMAs. As illustrated in Table S9 (Supporting Information), the effective “E/E+C/C” mode in Y6 affords a large V_E of 40 meV and “E/E-2” mode also demonstrates a good V_E of 35 meV. Compared with Y6, the “E/E” mode in CH22 possesses the largest V_E of 55 meV. Coincidentally, after central unit exten-

sion in CH52, both very small V_E s can be observed for two “dual E/C” modes, rendering the “E/E” mode with V_E of 47 meV as the most effective charge transfer pathway in crystal of CH52. Although CH72 exhibits only one stacking mode of “dual E/C” with the largest intermolecular potential of -271 kJ mol^{-1} , its V_E is quite small comparing to the preponderant packing modes in other three SMAs. The disappeared “E/E” stacking, which is usually regarded as an important charge transfer channel, may have a negative impact on charge transfer dynamics in resulting photovoltaic devices of CH72.

Figure S13 (Supporting Information) showed the X-ray diffraction patterns that were generated from single crystals of CH52 and CH72, which is roughly in accordance with the GIWAXs data in neat film. This indicates that the main packing modes of CH52 and CH72 in single crystals are largely maintained in their neat films. Although the regular molecular stackings existing in the single crystals may be not fully maintained in blended films of OSCs, the systematic analysis at single crystal levels still could draw the following inferences and revelations: 1) In CH-series SMAs, the stronger S-N secondary interaction can solidify molecular skeletons, thereby reducing molecular reorganization energies, prolonging exciton lifetimes, etc. 2) The 2D conjugated extension of central units, or different projected areas of central units, could have an great impact on the 3D topology of molecular stacking and also the specific stacking mode of molecules. As the central unit extending to the maximum, the most common “E/E” mode (one of the most important charge transfer channels in SMAs) even disappears, thus leaving the “dual E/C” mode completely dominates the stacking of CH70 and CH72. 3) The V_E between adjacent molecules is closely related to their packing mode. For example, even though the “dual E/C” packing mode of CH72 exhibits the largest intermolecular potential and the smallest π - π packing distance, its V_E is still very small. Therefore, the tuning/optimization of intermolecular packing modes should be crucially important if high-performance photovoltaic materials are expected. 4) More importantly, the well-balanced molecular packing modes involving both central and end units or suitable sizes of 2D central planes and end terminals need to be paid great attentions during molecular design. Specifically, although the central unit contributes greatly and even plays a leading role in building the 3D stacking network of SMAs, the “E/E” stacking of molecules still exert significant effects on obtaining efficient electron transfer (e.g., reaching a larger V_E), more red-shifted film absorption (“E/E” packing mode is more akin to the “head-to-head” J aggregates), etc.

2.3. Photovoltaic Performances

The different 2D conjugated extension of central planes has given rise to diverse molecular packing modes and networks of SMAs as expected, which should inevitably result in much different OSCs. Herein, OSCs with a conventional architecture were fabricated, in which PM6 donor was blended with Y6, CH22, CH52, and CH72 as light harvesting layers. Device fabrication details including device optimization and characterization were provided in Tables S10–S15 (Supporting Information). The current density-voltage (J - V) curves of the best OSC were presented in Figure 5a and derived parameters were summarized in Table 1.

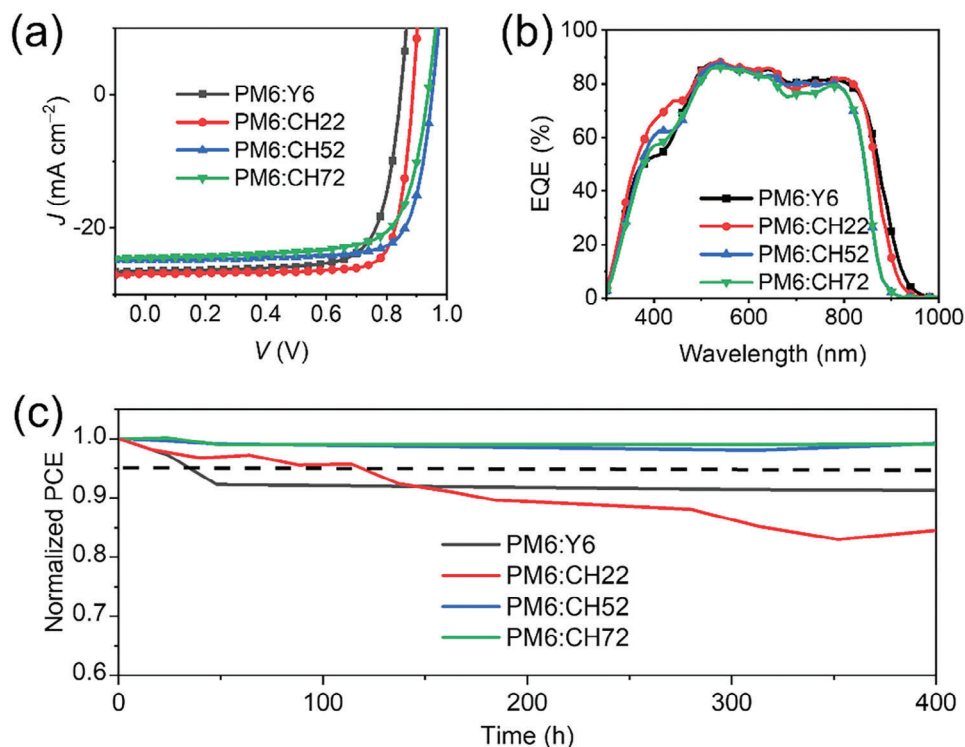


Figure 5. a) Current density-voltage curves of PM6:Y6, PM6:CH22, PM6:CH52, and PM6:CH72 based OSCs. b) The EQE spectra and integral J_{SC} values. c) Thermal stability of optimal devices.

For Y6-based photovoltaic device, a good PCE of 16.63% with a V_{OC} of 0.846 V, an excellent J_{SC} of 26.46 mA cm^{-2} and an FF of 74.27% is afforded. Note the PCE of the reference binary PM6: Y6 device is comparable to that in literature under similar conditions.^[2b] Benefiting from the optimized physico-chemical properties of CH22 at both single molecular and aggregated levels, a greatly improved PCE of 19.09% is yielded by the binary CH22-based device along with a good V_{OC} of 0.887 V, a J_{SC} of 26.78 mA cm^{-2} and an excellent FF of 80.34%. With the further expansion of central

unit in CH52, the V_{OC} of CH52-based OSCs reaches 0.951 V, however, the PCE decreases to 18.18% due to the good but far from ideal J_{SC} of 24.74 mA cm^{-2} and FF of 77.27%. In sharp contrast, when expanding central units to the maximum in CH72, the PCE of CH72-based OSCs decreases sharply, being only

16.55% with a V_{OC} of 0.937 V, a J_{SC} of 24.39 mA cm^{-2} and an FF of 72.41%. The external quantum efficiency (EQE) plots of Y6-, CH22-, CH52-, and CH72-based OSCs were exhibited in Figure 5b. The integrated current densities are 25.78, 25.81, 23.92, and 23.48 mA cm^{-2} , respectively, closing to those afforded by J - V tests. As shown in Figure 5 and Figure 2b, the EQE curve of CH52-based device is almost overlap with CH72-based device, whereas the absorption of CH52 neat film is blue-shift comparing to that of CH72. As shown in Figure S15b,c (Supporting Information), after blending with the donor PM6, the maximum absorption peaks of CH72 (9 nm) have a slightly greater blue shift than that of CH52 (7 nm), indicating stronger interaction between PM6 and CH72. In addition, the absorption variation of blend films of CH52 and CH72 is in good accordance with their EQE curves. To compare the miscibility between PM6 and SMAs,

Table 1. Optimized device performances based on PM6:Y6, PM6:CH22, PM6:CH52, and PM6:CH72 blended films.

Active Layer ^{a)}	V_{OC} [V]	J_{SC} [mA/cm^2]	J_{sc}^{EQE} ^{b)} [mA/cm^2]	FF [%]	PCE [%]
PM6:Y6	0.846 (0.843 ± 0.003)	26.46 (26.25 ± 0.38)	25.78	74.27 (74.05 ± 0.9)	16.63 (16.38 ± 0.19)
PM6:CH22	0.887 (0.885 ± 0.001)	26.78 (26.71 ± 0.09)	25.81	80.34 (80.16 ± 0.21)	19.09 (18.96 ± 0.06)
PM6:CH52	0.951 (0.951 ± 0.002)	24.74 (24.78 ± 0.08)	23.92	77.27 (76.44 ± 0.38)	18.18 (18.02 ± 0.06)
PM6:CH72	0.937 (0.937 ± 0.004)	24.39 (24.36 ± 0.09)	23.48	72.41 (71.56 ± 0.59)	16.55 (16.33 ± 0.09)

^{a)} Average parameters derived from 15 independent OSCs (Tables S12–S15, Supporting Information); ^{b)} Current densities by integrating EQE plots.

contact angles and derived Flory-Huggins interaction parameters (χ) were further evaluated. As shown in Figure S16 and Table S16 (Supporting Information), from Y6 to CH72, the gradually decreased $\chi_{D:A}$ have been observed (0.49 for Y6, 0.33 for CH22, 0.16 for CH52, 0.08 for CH72), demonstrating the enhanced D/A miscibility of CH72 with central planes enlarging. Note that the D/A miscibility of CH72 is larger than CH52, which corresponds to their EQE and absorption spectra of blend films. Although the stepwise blue-shifted absorption from Y6 to CH72 leads to gradually shrinking EQE spectra, the very similar EQE values can be observed in a wide range of 450–800 nm for Y6-, CH22- and CH52-based OSCs. However, the slightly smaller EQEs are afforded by CH72-based OSCs comparing to its other counterparts, which is caused by multiple factors, such as the relatively inferior exciton dissociation (Figure S17, Supporting Information), charge transport (Figure S18 and Table S17, Supporting Information) and recombination (Figure S19, Supporting Information) characteristics, etc. The intrinsic reason for the inferior dynamics in CH72-based devices may be assigned to the non-ideal molecular packing mode of CH72, which originates from the excessive 2D conjugated extension of central unit. In addition, OSCs based on CH22 and CH52 exhibit the obvious better PCEs than that of Y6, which mainly benefits from their enlarged V_{OC} and FF. Among them, the enlarged V_{OC} matches with the up-shifted LUMO of CH22 and CH52 comparing to that of Y6. And the larger FF could be assigned to their better molecular stacking behaviors and nanoscale morphologies (see detailed discussions below). As shown in Figure S20 and Table S18 (Supporting Information), the PCE of CH20, CH50, and CH70 are 16.78%, 13.80%, and 11.58%, respectively, which is slightly lower than their bromides, but also shows the same trend as CH22, CH52, and CH72.

Note that OSCs are a highly complicated system and their efficiencies are affected by multiple and tangled factors together. Therefore, the prediction of device efficiency or rational design of active layer materials are still quite challenging. However, the single crystal analysis should be a far from ideal but quite useful tools when attempting to reveal the structure-function relationship between structures of light-harvesting molecules and the photovoltaic performances of resulting OSCs. Herein, based on our systematic crystal analysis, the alkyl chains on molecular backbones are mainly distributed in voids in high-performance CH-SMA systems, thus leaving the relative size of central units and end terminals largely determines the stacking modes and topology structures of 3D molecular packing network. Especially, when the ratio of central plane projected area (S_C)/end terminal projected area (S_E) is no more than 3, the SMAs-based OSCs usually show excellent efficiencies (see the summary in Table S19, Supporting Information). The inner reasons may be ascribed to their specific intermolecular modes. For instance, the widely existed “E/E” modes that benefitting for efficient charge transfer greatly, may vanish from sight if S_C/S_E is much larger than 3, such as CH70 and CH72. Furthermore, the multiple and well-balanced molecular packing modes involving both central and end units may be observed and further contribute to a more preferred 3D intermolecular packing network when S_C/S_E locating at a proper. Of course, the imbedded heteroatoms on central units (like nitrogen, sulfur, halogens, etc.) may provide much more enhanced interaction of central planes through intermolecular non-

covalent bonds, thus making the S_C/S_E deviate from the suitable range.

It is worth noting that PCEs of CH52- and CH72-based OSCs could be maintained above 95% comparing to the initial PCEs after 400 h under heat treatment at 65 °C (Figure 5c). The relatively good storage and thermal stabilities could be correlated to the better morphology stability of active layers, which may originate from their unique intermolecular packing modes of CH52 and CH72 with stronger intermolecular interactions (indicated by their large intermolecular potentials).

2.4. Morphology and Energy Loss Analysis

As it was fully discussed, in OSCs, the morphology of active layers is crucial for influencing the dynamics of charge transfer/transport/recombination dynamics and photovoltaic performances. To unveil the morphology characteristics of active layers, we performed atomic force microscopy (AFM) tests (Figure 6; Figure S21, Supporting Information). As shown in Figure S21 (Supporting Information), all the blended films display a smooth surface morphology indicated by the root-mean square (RMS) roughness values of 0.70 for PM6:Y6, 0.93 for PM6:CH22, 1.17 for PM6:CH52, and 0.97 nm for PM6:CH72. In aspect of the phase images (Figure 5e–h), all four blended films exhibit fiber-like domains, which are known to instrumental in enhancing charge transport within OSCs.^[23] Statistical analysis of nanofiber dimensions, as depicted in Figure 5h and Figure S22 (Supporting Information), shows a progressive enlargement of fiber size: 8 for Y6, 11 for CH22, 14 for CH52, and 14 nm for CH72, suggesting that extending the central units’ planar size potentially enhances molecular crystallinity and adjusts the sizes of phase domains. Meanwhile, the fiber size of the CH-series molecule in all blended films have the ranges from 10 to 20 nm, which is favorable for facilitating high charge mobility and avail charge transport. However, these advantages are not demonstrated in the device of CH72, which may be due to the vanishing of “E/E” modes that benefitting for efficient charge transfer greatly. Thereafter, the effect of stepwise 2D conjugated extension of central planes on molecular packings in blended films was further investigated by performing GIWAXS measurements (Figure 6c; Figure S23 and Table S20, Supporting Information). When compared to their respective neat films, in the blended films with PM6 donor, the sharp (010) diffraction peaks still exist in OOP directions, implying that the preferential π - π stacking of face on orientation has been well kept. The (010) diffraction peaks in OOP direction for Y6, CH22, CH52, and CH72 blended films locate at 1.74, 1.70, 1.72, and 1.73 Å⁻¹, which correspond to the π - π stacking distances ($d_{\pi-\pi}$) of 3.60, 3.70, 3.66, and 3.64 Å, respectively. The slightly larger $d_{\pi-\pi}$ s for three CH-series SMAs comparing to that of Y6 should be ascribed to their greatly enlarged alkyl substituents on both nitrogen atoms. However, an obviously decreased $d_{\pi-\pi}$ from CH22 to CH72 should be caused by the enhanced intermolecular packing strength with the plane size of central units increasing, which agrees well with the data from AFM images and single crystal.

With the aim of revealing the potential correlation between plane size of central units of SMAs and energy loss of resulting OSCs, a comprehensive analysis has been conducted to

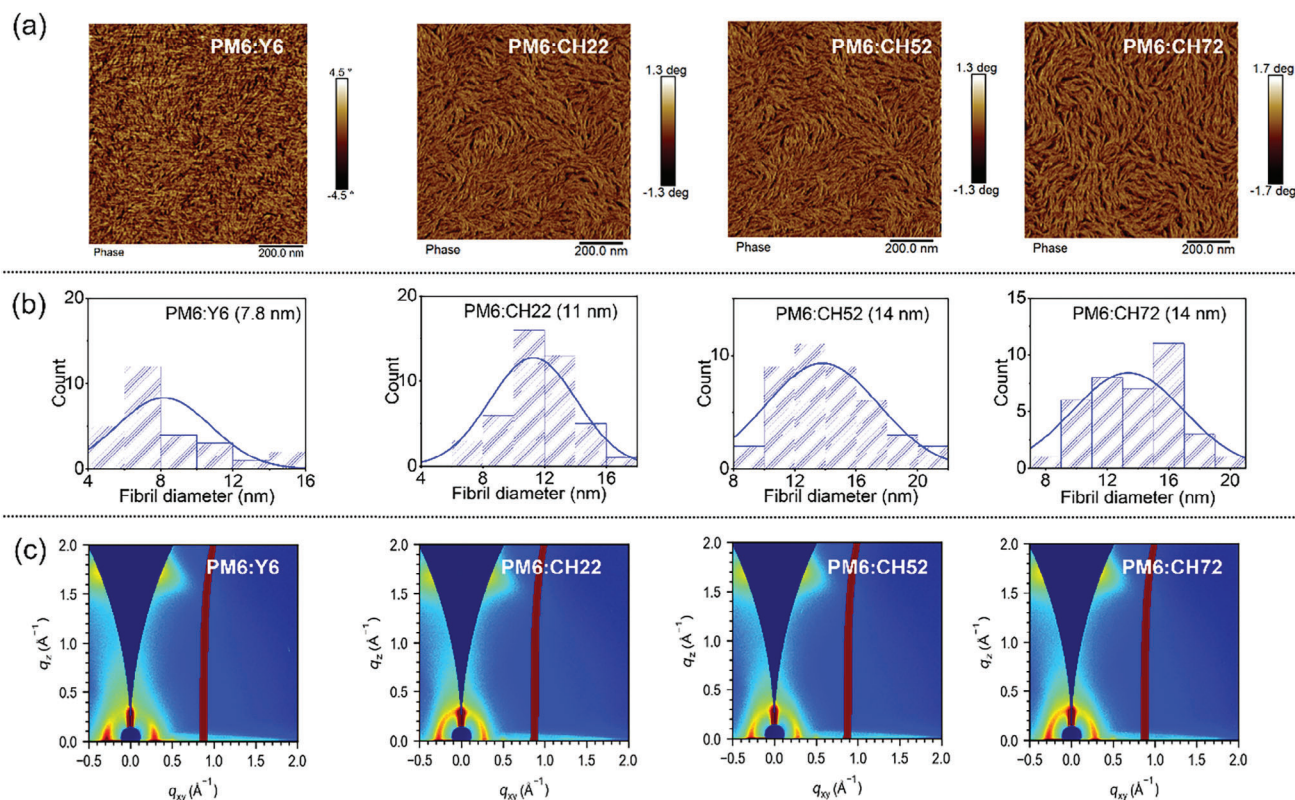


Figure 6. a) AFM phase images of PM6:Y6, PM6:CH22, PM6:CH52, and PM6:CH72 blended films. b) The statistical distribution of fibril diameter derived from AFM phase images. c) 2D GIWAXS patterns of blended films.

quantitatively assess the energy losses in PM6:SMA-based devices (see Supporting Information for the detailed method of measurements, Figure S24, Supporting Information).^[15b,24] As illustrated in Table S21 (Supporting Information), the energy losses were greatly decreased in CH-series SMA-based devices comparing to that of Y6 (0.561 for Y6, 0.516 for CH22, 0.501 for CH52, and 0.525 eV for CH72), especially for the most concerned non-radiative recombination losses (0.230 for Y6, 0.170 for CH22, 0.104 for CH52, and 0.098 eV for CH72). This may be attributed to the enhanced molecular crystallinity and fine tune phase domain sizes through central unit extension. Note that PM6:CH52 based OSCs afford the smallest energy loss of 0.501 eV among the four SMA systems, demonstrating that charge recombination in OSCs could be successfully suppressed by tuning the plane size of central units of SMAs.

3. Conclusion

A series of high-performance SMAs were constructed with gradually enlarged central unit sizes comparing to their Y6 counterpart, for example the projected area of central units is ≈ 8.5 for Y6, ≈ 15.3 for CH22, ≈ 23.7 for CH52, and $\approx 30.6 \text{ \AA}^2$ for CH72. A comprehensive investigation at both single molecular and solid-state levels has been performed with the aim of exploring the proper size of 2D central planes and made a correlation to the characteristic 3D intermolecular packing networks, with even quite different efficiencies of the CH-series SMAs. Several new cognitions

that may benefit for further rational molecular design have been disclosed as following: 1) At the single molecular level, 2D conjugated extension of central unit in CH-series SMAs will bring advantages such as reduced reorganization energies, prolonged exciton lifetimes, decreased exciton binding energies, etc. 2) When transforming to packing states from single molecule, the desired properties of SMAs in gas phases may be not fully maintained or fatal due to the complexity of organic molecule stacking. For example, the gradually blue-shifted absorption in film states from CH22 to CH72 can be observed beyond thought in spite of their almost identical absorption in diluted solutions. This could be caused by the different packing modes of SMAs that are more akin to J- or H-aggregates. 3) With the central plane size extended to the maximum (like CH72), the huge central unit may provide an overwhelming driving force to prompt the formation of packing modes dominated by central units. In extreme cases, the most common “E/E” mode even disappears completely, whereas the “E/E” stacking mode is usually regarded as an important charge transfer channel. 4) The V_E between adjacent molecules is closely related to their packing mode. Even though the “dual E/C” packing mode of CH72 exhibits the largest intermolecular potential and the smallest π - π packing distance, its V_E is still very small. Therefore, the tuning/optimization of intermolecular packing modes should be crucially important if high-performance photovoltaic materials are expected. 5) The great significance of multiple and well-balanced molecular packing modes involves both central and end units (or with a proper ratio of S_C/S_E at no more

than 3) in determining a more preferred 3D intermolecular packing network for SMAs. By exploring the limit size of 2D central planes, the possible structural profiles of central unit that well-meet the design criterion of high-performance SMAs have been elusive, e.g. candidates with suitable central unit size but sufficient heteroatoms instead of directly extending 2D conjugated planes to the maximum. Our work would likely stimulate further exploration on novel SMAs with 2D conjugated central planes beyond doubt and may boost the record efficiency of OSCs further.

Supporting Information

Supporting Information is available from the Wiley Online Library or from the author.

Acknowledgements

The authors gratefully acknowledge the financial support from Ministry of Science and Technology of the People's Republic of China (National Key R&D Program of China, 2022YFB4200400, 2019YFA0705900, 2023YFE0210400) and National Natural Science Foundation of China (22204119, 21935007, 52025033, 22361132530, 22309090), 111 Project (B12015), Tianjin city (20JCZDJC00740). The authors gratefully acknowledge the cooperation of the beamline scientists at BSRF-1W1A beamline (Beijing).

Conflict of Interest

The authors declare no conflict of interest.

Author Contributions

X.B. and X.C. contributed equally to this work. The synthetic works were carried out by X.B.; the device optimizations and measurements were carried out by X.C.; T.H. performed the DFT calculations. Y.C. and Z.Y. conceived and directed the study. Y.G., B.K., X.W., C.L. et al. helped to analyze the data and commented on the manuscript.

Data Availability Statement

The data that support the findings of this study are available from the corresponding author upon reasonable request.

Keywords

limit size exploration, molecular packing, solar cell, structure-function correlation

Received: February 9, 2024

Revised: March 6, 2024

Published online:

- [1] a) C. W. Tang, *Appl. Phys. Lett.* **1986**, *48*, 183; b) G. Yu, J. Gao, J. C. Hummelen, F. Wudl, A. J. Heeger, *Science* **1995**, *270*, 1789; c) L. Meng, Y. Zhang, X. Wan, C. Li, X. Zhang, Y. Wang, X. Ke, Z. Xiao, L. Ding, R. Xia, H.-L. Yip, Y. Cao, Y. Chen, *Science* **2018**, *361*, 1094; d) J. Wang, Z.

- Zheng, P. Bi, Z. Chen, Y. Wang, X. Liu, S. Zhang, X. Hao, M. Zhang, Y. Li, J. Hou, *Natl. Sci. Rev.* **2023**, *10*, nwad085; e) Z. Jia, S. Qin, L. Meng, Q. Ma, I. Angunawela, J. Zhang, X. Li, Y. He, W. Lai, N. Li, H. Ade, C. J. Brabec, Y. Li, *Nat. Commun.* **2021**, *12*, 178; f) J. Zhang, H. S. Tan, X. Guo, A. Facchetti, H. Yan, *Nat. Energy* **2018**, *3*, 720; g) Y. Liang, D. Zhang, Z. Wu, T. Jia, L. Lüer, H. Tang, L. Hong, J. Zhang, K. Zhang, C. J. Brabec, N. Li, F. Huang, *Nat. Energy* **2022**, *7*, 1180; h) F. Lin, K. Jiang, W. Kaminsky, Z. Zhu, A. K. Jen, *J. Am. Chem. Soc.* **2020**, *142*, 15246; i) Y. Liu, T. P. Russell, *Acc. Chem. Res.* **2022**, *55*, 1097.
- [2] a) Y. Lin, J. Wang, Z.-G. Zhang, H. Bai, Y. Li, D. Zhu, X. Zhan, *Adv. Mater.* **2015**, *27*, 1170; b) J. Yuan, Y. Zhang, L. Zhou, G. Zhang, H.-L. Yip, T.-K. Lau, X. Lu, C. Zhu, H. Peng, P. A. Johnson, M. Leclerc, Y. Cao, J. Ulanski, Y. Li, Y. Zou, *Joule* **2019**, *3*, 1140; c) L. Zhu, M. Zhang, J. Xu, C. Li, J. Yan, G. Zhou, W. Zhong, T. Hao, J. Song, X. Xue, Z. Zhou, R. Zeng, H. Zhu, C.-C. Chen, R. C. I. MacKenzie, Y. Zou, J. Nelson, Y. Zhang, Y. Sun, F. Liu, *Nat. Mater.* **2022**, *21*, 656; d) K. Jiang, J. Zhang, C. Zhong, F. R. Lin, F. Qi, Q. Li, Z. Peng, W. Kaminsky, S.-H. Jang, J. Yu, X. Deng, H. Hu, D. Shen, F. Gao, H. Ade, M. Xiao, C. Zhang, A. K. Y. Jen, *Nat. Energy* **2022**, *7*, 1076; e) C. Duan, L. Ding, *Sci. Bull.* **2020**, *65*, 1231; f) Z. Zheng, J. Wang, P. Bi, J. Ren, Y. Wang, Y. Yang, X. Liu, S. Zhang, J. Hou, *Joule* **2022**, *6*, 171; g) C. Dou, X. Long, Z. Ding, Z. Xie, J. Liu, L. Wang, *Angew. Chem., Int. Ed.* **2016**, *55*, 1436; h) S. Li, C. He, T. Chen, J. Zheng, R. Sun, J. Fang, Y. Chen, Y. Pan, K. Yan, C.-Z. Li, M. Shi, L. Zuo, C.-Q. Ma, J. Min, Y. Liu, H. Chen, *Energy Environ. Sci.* **2023**, *16*, 2262; i) Y. Ma, M. Zhang, S. Wan, P. Yin, P. Wang, D. Cai, F. Liu, Q. Zheng, *Joule* **2021**, *5*, 197; j) K. Chong, X. Xu, H. Meng, J. Xue, L. Yu, W. Ma, Q. Peng, *Adv. Mater.* **2022**, *34*, 2109516; k) Y. Liu, Z. Zhang, S. Feng, M. Li, L. Wu, R. Hou, X. Xu, X. Chen, Z. Bo, *J. Am. Chem. Soc.* **2017**, *139*, 3356; l) H. Sun, B. Liu, Y. Ma, J.-W. Lee, J. Yang, J. Wang, Y. Li, B. Li, K. Feng, Y. Shi, B. Zhang, D. Han, H. Meng, L. Niu, B. J. Kim, Q. Zheng, X. Guo, *Adv. Mater.* **2021**, *33*, 2102635; m) Y. Sun, L. Nian, Y. Kan, Y. Ren, Z. Chen, L. Zhu, M. Zhang, H. Yin, H. Xu, J. Li, X. Hao, F. Liu, K. Gao, Y. Li, *Joule* **2022**, *6*, 2835; n) Z. Zhang, Y. Li, G. Cai, Y. Zhang, X. Lu, Y. Lin, *J. Am. Chem. Soc.* **2020**, *142*, 18741; o) H. Wang, C. Cao, H. Chen, H. Lai, C. Ke, Y. Zhu, H. Li, F. He, *Angew. Chem., Int. Ed.* **2022**, *61*, 202201844.
- [3] a) S. Zhang, F. Ye, X. Wang, R. Chen, H. Zhang, L. Zhan, X. Jiang, Y. Li, X. Ji, S. Liu, M. Yu, F. Yu, Y. Zhang, R. Wu, Z. Liu, Z. Ning, D. Neher, L. Han, Y. Lin, H. Tian, W. Chen, M. Stolterfoht, L. Zhang, W.-H. Zhu, Y. Wu, *Science* **2023**, *380*, 404; b) J. J. Yoo, G. Seo, M. R. Chua, T. G. Park, Y. Lu, F. Rotermund, Y. K. Kim, C. S. Moon, N. J. Jeon, J. P. Correa-Baena, V. Bulovic, S. S. Shin, M. G. Bawendi, J. Seo, *Nature* **2021**, *590*, 587; c) H. Lu, W. Liu, G. Ran, Z. Liang, H. Li, N. Wei, H. Wu, Z. Ma, Y. Liu, W. Zhang, X. Xu, Z. Bo, *Angew. Chem., Int. Ed.* **2023**, *62*, 202314420; d) B. Pang, C. Liao, X. Xu, L. Yu, R. Li, Q. Peng, *Adv. Mater.* **2023**, *35*, 2300631; e) L. Rao, X. Meng, S. Xiao, Z. Xing, Q. Fu, H. Wang, C. Gong, T. Hu, X. Hu, R. Guo, Y. Chen, *Angew. Chem., Int. Ed.* **2021**, *60*, 14693; f) X. Chin, D. Turkay, J. A. Steele, S. Tabean, S. Eswara, M. Mensi, P. Fiala, C. M. Wolff, A. Paracchino, K. Artuk, D. Jacobs, Q. Guesnay, F. Sahli, G. Andreatta, M. Boccard, Q. Jeangros, C. Ballif, *Science* **2023**, *381*, 59.
- [4] a) X. Yan, J. Wu, J. Lv, L. Zhang, R. Zhang, X. Guo, M. Zhang, *J. Mater. Chem. A* **2022**, *10*, 15605; b) L. Zhu, J. Zhang, Y. Guo, C. Yang, Y. Yi, Z. Wei, *Angew. Chem., Int. Ed.* **2021**, *60*, 15348; c) W. Zhu, A. P. Spencer, S. Mukherjee, J. M. Alzola, V. K. Sangwan, S. H. Amsterdam, S. M. Swick, L. O. Jones, M. C. Heiber, A. A. Herzog, G. Li, C. L. Stern, D. M. DeLongchamp, K. L. Kohlstedt, M. C. Hersam, G. C. Schatz, M. R. Wasielewski, L. X. Chen, A. Facchetti, T. J. Marks, *J. Am. Chem. Soc.* **2020**, *142*, 14532; d) A. Gavezzotti, G. Filippini, *J. Phys. Chem.* **1994**, *98*, 4831; e) H. Yang, C. Cui, Y. Li, *Acc. Chem. Res.* **2021**, *2*, 986; f) Z. Wang, Y. Zhang, J. Zhang, Z. Wei, W. Ma, *Adv. Energy Mater.* **2016**, *6*, 1502456; g) Y. Wei, Z. Chen, G. Lu, N. Yu, C. Li, J. Gao, X. Gu, X. Hao, G. Lu, Z. Tang, J. Zhang, Z. Wei, X. Zhang, H. Huang, *Adv. Mater.* **2022**, *34*, 2204718; h) L. D. Whalley, P. van Gerwen, J. M. Frost, S. Kim, S. N. Hood, A. Walsh, *J. Am. Chem. Soc.* **2021**, *143*, 9123;

- i) J. Lin, M. Lai, L. Dou, C. S. Kley, H. Chen, F. Peng, J. Sun, D. Lu, S. A. Hawks, C. Xie, F. Cui, A. P. Alivisatos, D. T. Limmer, P. Yang, *Nat. Mater.* **2018**, *17*, 261.
- [5] D. Beljonne, G. Pourtois, C. Silva, E. Hennebicq, L. M. Herz, R. H. Friend, G. D. Scholes, S. Setayesh, K. Müllen, J. L. Brédas, *Proc. Natl. Acad. Sci. USA* **2002**, *99*, 10982.
- [6] K. Feron, X. Zhou, W. J. Belcher, P. C. Dastoor, *J. Appl. Phys.* **2012**, *111*, 044510.
- [7] K. Nakano, Y. Chen, B. Xiao, W. Han, J. Huang, H. Yoshida, E. Zhou, K. Tajima, *Nat. Commun.* **2019**, *10*, 2520.
- [8] a) N. F. Mott, *Trans. Faraday Soc.* **1938**, *34*, 500; b) S. Li, Z. Xiao, J.-J. Li, Z.-Y. Hu, Y. Yang, B. Kan, D.-S. Guo, X. Wan, Z. Yao, C. Li, Y. Chen, *Sci. China Chem.* **2022**, *66*, 195; c) L. Meng, H.-H. Gao, S. Wu, Y. Sun, X. Wan, Y. Yang, J. Wang, Z. Guo, H. Chen, C. Li, Y. Chen, *Sci. China Mater.* **2021**, *64*, 2388.
- [9] I. Ramirez, M. Causa', Y. Zhong, N. Banerji, M. Riede, *Adv. Energy Mater.* **2018**, *8*, 1703551.
- [10] a) H. Chen, Y. Zou, H. Liang, T. He, X. Xu, Y. Zhang, Z. Ma, J. Wang, M. Zhang, Q. Li, C. Li, G. Long, X. Wan, Z. Yao, Y. Chen, *Sci. China Chem.* **2022**, *65*, 1362; b) Z. Luo, T. Liu, Y. Xiao, T. Yang, Z. Chen, G. Zhang, C. Zhong, R. Ma, Y. Chen, Y. Zou, X. Lu, H. Yan, C. Yang, *Nano Energy* **2019**, *66*, 104146; c) C. Li, J. Zhou, J. Song, J. Xu, H. Zhang, X. Zhang, J. Guo, L. Zhu, D. Wei, G. Han, J. Min, Y. Zhang, Z. Xie, Y. Yi, H. Yan, F. Gao, F. Liu, Y. Sun, *Nat. Energy* **2021**, *6*, 605; d) L. Wang, Q. An, L. Yan, H.-R. Bai, M. Jiang, A. Mahmood, C. Yang, H. Zhi, J.-L. Wang, *Energy Environ. Sci.* **2022**, *15*, 320; e) Y. Jiang, Y. Li, F. Liu, W. Wang, W. Su, W. Liu, S. Liu, W. Zhang, J. Hou, S. Xu, Y. Yi, X. Zhu, *Nat. Commun.* **2023**, *14*, 5079; f) J. Wan, Y. Wu, R. Sun, J. Qiao, X. Hao, J. Min, *Energy Environ. Sci.* **2022**, *15*, 5192; g) M. Zhang, L. Zhu, G. Zhou, T. Hao, C. Qiu, Z. Zhao, Q. Hu, B. W. Larson, H. Zhu, Z. Ma, Z. Tang, W. Feng, Y. Zhang, T. P. Russell, F. Liu, *Nat. Commun.* **2021**, *12*, 309; h) Y. Shi, Y. Chang, K. Lu, Z. Chen, J. Zhang, Y. Yan, D. Qiu, Y. Liu, M. A. Adil, W. Ma, X. Hao, L. Zhu, Z. Wei, *Nat. Commun.* **2022**, *13*, 3256.
- [11] Z. Yao, X. Wan, C. Li, Y. Chen, *Acc. Chem. Res.* **2023**, *4*, 772.
- [12] Y. Zou, H. Chen, X. Bi, X. Xu, H. Wang, M. Lin, Z. Ma, M. Zhang, C. Li, X. Wan, G. Long, Y. Zhaoyang, Y. Chen, *Energy Environ. Sci.* **2022**, *15*, 3519.
- [13] H. Liang, X. Bi, H. Chen, T. He, Y. Lin, Y. Zhang, K. Ma, W. Feng, Z. Ma, G. Long, C. Li, B. Kan, H. Zhang, O. A. Rakitin, X. Wan, Z. Yao, Y. Chen, *Nat. Commun.* **2023**, *14*, 4707.
- [14] a) G. Zhang, X.-K. Chen, J. Xiao, P. C. Y. Chow, M. Ren, G. Kupgan, X. Jiao, C. C. S. Chan, X. Du, R. Xia, Z. Chen, J. Yuan, Y. Zhang, S. Zhang, Y. Liu, Y. Zou, H. Yan, K. S. Wong, V. Coropceanu, N. Li, C. J. Brabec, J.-L. Bredas, H.-L. Yip, Y. Cao, *Nat. Commun.* **2020**, *11*, 3943; b) X. Zhang, C. Li, J. Xu, R. Wang, J. Song, H. Zhang, Y. Li, Y.-N. Jing, S. Li, G. Wu, J. Zhou, X. Li, Y. Zhang, X. Li, J. Zhang, C. Zhang, H. Zhou, Y. Sun, Y. Zhang, *Joule* **2022**, *6*, 444.
- [15] a) J. Benduhn, K. Tvingstedt, F. Piersimoni, S. Ullbrich, Y. Fan, M. Tropiano, K. A. McGarry, O. Zeika, M. K. Riede, C. J. Douglas, S. Barlow, S. R. Marder, D. Neher, D. Spoltore, K. Vandewal, *Nat. Energy* **2017**, *2*, 17053; b) X.-K. Chen, D. Qian, Y. Wang, T. Kirchartz, W. Tress, H. Yao, J. Yuan, M. Hülsbeck, M. Zhang, Y. Zou, Y. Sun, Y. Li, J. Hou, O. Inganäs, V. Coropceanu, J.-L. Bredas, F. Gao, *Nat. Energy* **2021**, *6*, 799; c) F. D. Eisner, M. Azzouzi, Z. Fei, X. Hou, T. D. Anthopoulos, T. J. S. Dennis, M. Heeney, J. Nelson, *J. Am. Chem. Soc.* **2019**, *141*, 6362; d) D. Qian, Z. Zheng, H. Yao, W. Tress, T. R. Hopper, S. Chen, S. Li, J. Liu, S. Chen, J. Zhang, X.-K. Liu, B. Gao, L. Ouyang, Y. Jin, G. Pozina, I. A. Buyanova, W. M. Chen, O. Inganäs, V. Coropceanu, J.-L. Bredas, H. Yan, J. Hou, F. Zhang, A. A. Bakulin, F. Gao, *Nat. Mater.* **2018**, *17*, 703; e) F. Huang, T. He, M. Li, L. Meng, W. Feng, H. Liang, Y. Zhou, X. Wan, C. Li, G. Long, Z. Yao, Y. Chen, *Chem. Mater.* **2022**, *34*, 6009; f) A. Ashokan, T. Wang, M. K. Ravva, J.-L. Brédas, *J. Mater. Chem. C* **2018**, *6*, 13162.
- [16] T. Chen, S. Li, Y. Li, Z. Chen, H. Wu, Y. Lin, Y. Gao, M. Wang, G. Ding, J. Min, Z. Ma, H. Zhu, L. Zuo, H. Chen, *Adv. Mater.* **2023**, *35*, 2300400.
- [17] H. Wang, T. Liu, J. Zhou, D. Mo, L. Han, H. Lai, H. Chen, N. Zheng, Y. Zhu, Z. Xie, F. He, *Adv. Sci.* **2020**, *7*, 1903784.
- [18] X. Wan, C. Li, M. Zhang, Y. Chen, *Chem. Soc. Rev.* **2020**, *49*, 2828.
- [19] M. F. Huang, Y. Zeng, G. C. Han, Y. P. Yi, *J. Phys. Chem. C* **2023**, *127*, 5597.
- [20] a) F. C. Spano, *Acc. Chem. Res.* **2010**, *43*, 429; b) T. Li, J. Benduhn, Z. Qiao, Y. Liu, Y. Li, R. Shivhare, F. Jaiser, P. Wang, J. Ma, O. Zeika, D. Neher, S. C. B. Mannsfeld, Z. Ma, K. Vandewal, K. Leo, *J. Phys. Chem. Lett.* **2019**, *10*, 2684; c) Q. Zhao, H. Lai, H. Chen, H. Li, F. He, *J. Mater. Chem. A* **2021**, *9*, 1119.
- [21] P. Müller-Buschbaum, *Adv. Mater.* **2014**, *26*, 7692.
- [22] H. Chen, H. Liang, Z. Guo, Y. Zhu, Z. Zhang, Z. Li, X. Cao, H. Wang, W. Feng, Y. Zou, L. Meng, X. Xu, B. Kan, C. Li, Z. Yao, X. Wan, Z. Ma, Y. Chen, *Angew. Chem., Int. Ed.* **2022**, *61*, 202209580.
- [23] S. Li, L. Zhan, N. Yao, X. Xia, Z. Chen, W. Yang, C. He, L. Zuo, M. Shi, H. Zhu, X. Lu, F. Zhang, H. Chen, *Nat. Commun.* **2021**, *12*, 4627.
- [24] a) U. Rau, B. Blank, T. C. M. Muller, T. Kirchartz, *Phys. Rev. Appl.* **2017**, *7*, 044016; b) J. Yuan, H. Zhang, R. Zhang, Y. Wang, J. Hou, M. Leclerc, X. Zhan, F. Huang, F. Gao, Y. Zou, Y. Li, *Chem* **2020**, *6*, 2147; c) Y. Sun, H.-H. Gao, S. Wu, L. Meng, X. Wan, M. Li, Z. Ma, Z. Guo, S. Li, H. Zhang, C. Li, Y. Chen, *Sci. China Chem.* **2021**, *64*, 608; d) W. Zhu, J. M. Alzola, T. J. Aldrich, K. L. Kohlstedt, D. Zheng, P. E. Hartnett, N. D. Eastham, W. Huang, G. Wang, R. M. Young, G. C. Schatz, M. R. Wasielewski, A. Facchetti, F. S. Melkonyan, T. J. Marks, *ACS Energy Lett.* **2019**, *4*, 2695.